Radiation Dosimetry of ^{99m}Tc-Labeled C225 in Patients with Squamous Cell Carcinoma of the Head and Neck

Naomi R. Schechter, MD[1]; Richard E. Wendt III, PhD[2]; David J. Yang, PhD[2]; Ali Azhdarinia, MS[2]; William D. Erwin, MS[2]; Anne M. Stachowiak, AAS[2]; Lyle D. Broemeling, PhD[3]; E. Edmund Kim, MD[2]; James D. Cox, MD[1]; Donald A. Podoloff, MD[2]; and K. Kian Ang, MD, PhD[1]

[1]Division of Radiation Oncology, University of Texas M.D. Anderson Cancer Center, Houston, Texas; [2]Division of Diagnostic Imaging, University of Texas M.D. Anderson Cancer Center, Houston, Texas; and [3]Division of Biostatistics, University of Texas M.D. Anderson Cancer Center, Houston, Texas

This study assessed the radiation dosimetry of ^{99m}Tc-labeled ethylene dicysteine (EC) C225 (EC-C225), a promising radioligand for functional tumor imaging. **Methods:** Whole-body scanning was performed on 6 patients with head and neck squamous cell carcinoma up to 24 h after administration of ^{99m}Tc-EC-C225. Alternate patients who had been randomized to receive C225 in a phase III trial received ^{99m}Tc-EC-C225 before their 20-mg test dose or after their 400 mg/m^2 loading dose of unlabeled C225 (patients 1/3/5 and 2/4/6, respectively). Radiation dosimetry was assessed using the MIRD method. **Results:** The critical organ was the kidney, with an average radiation-absorbed dose for all 6 patients of 0.0274 mGy/MBq. The average total-body absorbed dose was 0.0022 mGy/MBq (0.243 cGy/1,110 MBq). **Conclusion:** The new radiopharmaceutical ^{99m}Tc-EC-C225 appears to have reasonable dosimetric properties for a diagnostic nuclear medicine agent. Correlation of the imaging results with clinical findings is the next step.

Key Words: epidermal growth factor receptor; dosimetry; imaging; technetium; C225

J Nucl Med 2004; 45:1683–1687

One factor indicating a poor prognosis in patients with squamous cell carcinoma of the head and neck is upregulation of the epidermal growth factor receptor (EGFR) (*1–8*). Antibody therapy, in a single modality or in combination with radiation or chemotherapy, directed against EGFR-expressing tumors (e.g., C225) is under investigation in the laboratory and clinic (*9–23*). Proper selection of patients for such therapy would likely improve the therapeutic ratio. Unfortunately, squamous cell carcinoma of the head and neck can grow quite large, and biopsy of a single portion of a tumor may not be representative.

Received Mar. 19, 2004; revision accepted Jun. 2, 2004.

For correspondence or reprints contact: Naomi Schechter, MD, Department of Radiation Oncology, University of Texas M.D. Anderson Cancer Center, 1515 Holcombe Blvd., Box 97, Houston, TX 77030.

E-mail: nschecht@mdanderson.org

Our goal was to develop a noninvasive imaging procedure that could detect tumors that express EGFR. For this purpose, ^{99m}Tc-labeled C225 was synthesized at our institution with an ethylene dicysteine (EC)–based chelation technique (EC-C225) (*24*). Technetium was chosen because of its low energy, short half-life (6 h), and low cost and because tumor does not take up free ^{99m}Tc, unlike another candidate radionuclide, ^{111}In. EC is a relatively small molecule (molecular weight, 260), which conjugates to C225 (molecular weight, >30,000). The chelation procedure does not affect the affinity of C225 for tumor or the cytotoxicity profile of C225 (*24*). The labeling procedure is easy and inexpensive, and the necessary γ-camera is commonly available.

Six patients already scheduled to receive concomitant treatment with radiation therapy and C225 (IMCL CP02-9815; ImClone Systems, Inc.) consented to undergo the experimental imaging with ^{99m}Tc-EC-C225. Based on the recommendation of the Food and Drug Administration, half the patients were given their loading dose of unlabeled C225 before the administration of ^{99m}Tc-EC-C225. Clinical radiation dosimetry data are reported below.

MATERIALS AND METHODS

Radiosynthesis of ^{99m}Tc-EC-C225

The linker EC was prepared in a 2-step synthesis according to methods described by Blondeau et al. (*25*) and Ratner et al. (*26*). Briefly, cysteine-HCl (41.52 g) was dissolved in water (106 mL). To this, formaldehyde was added (26.1 mL), and the reaction mixture was stirred overnight at room temperature. Pyridine (26.6 mL) was then added and the precipitate formed. The crystals were separated and washed with ethanol (54 mL) for 25 min at room temperature, then filtered with a Buchner funnel. The crystals were triturated with petroleum ether (150 mL), again filtered, and then lyophilized for 3 d. The precursor, L-thiazolidine-4-carboxylic acid (melting point, 195°C; reported, 196°C–197°C), was used for synthesis of EC. The precursor (22 g) was dissolved in liquid ammonia (200 mL) and refluxed. Sodium metal was added until a persistent blue color appeared. Ammonium chloride was added to

the blue solution, and then the solvents were evaporated to dryness. The residue was dissolved in water (200 mL), and the pH was adjusted to 2 by adding concentrated hydrochloric acid. A precipitate was formed as a result of pH adjustment to 2. The solid was filtered and washed with water (500 mL). The solid, EC (melting point, 247°C; reported, 251°C–253°C), was dried in a calcium chloride desiccator. The structure was confirmed by ^{1}H nuclear magnetic resonance and fast-atom-bombardment mass spectroscopy (mass-to-charge ratio, 268; molecule parent ion, 100).

Clinical grade anti-EGFR mAb C225 (IMC-C225) was obtained from ImClone Systems, Inc. C225 (20 mg) was stirred with EC (28.8 mg, 0.11 mmol in 1.4 mL of 1N $NaHCO_3$), *N*-hydroxysulfosuccinimide (23.3 mg, 0.11 mmol), and 1-ethyl-3-(3-dimethylaminopropyl)carbodiimide-HCl (16.6 mg, 0.09 mmol). After dialysis, 17 mg of EC-C225 were obtained. $Na^{99m}TcO_4$ (3,700 MBq) was added to a vial containing 1 mg of EC-C225 and 100 μg of $SnCl_2$, and the product was purified with a G-25 column and eluted with phosphate-buffered saline, yielding 2,960 MBq of ^{99m}Tc-EC-C225. Radiochemical purity was assessed by high-performance liquid chromatography (HPLC), using a sodium iodide detector and ultraviolet detector (254 nm). HPLC was performed on a gel permeation column (Biosep SEC-S3000, 7.8 × 300 mm; Phenomenex) eluted with 0.1% LiBr in pH 7.4 phosphate-buffered saline (10 mmol/L) at a flow rate of 1.0 mL/min. The retention time for ^{99m}Tc-EC-C225 was 10.2–10.6 min. In some samples, there was a second small peak (<10%) at 7.5 min, which might have been a lower-molecular-weight antibody. Radiochemical purity for ^{99m}Tc-EC-C225 was 90%–100%. Specific activity was 74 GBq/μmol.

An immunoassay (Western blot and immunoprecipitation) and cell proliferation assays were used to examine the integrity of EC-C225. Western blot analysis was also performed on A431 (high EGFR expression, positive control), MDA231 (medium EGFR expression), and MDA453 (poor EGFR expression, negative control) cell lines. DiFi cells are known to undergo apoptosis when exposed to C225 in culture; thus, they were used for cell viability assays. Cell viability was determined by measuring the optical absorbance of cell lysate at a wavelength of 595 nm and normalizing the value with the corresponding untreated cells. Our previous studies showed no marked changes in EGFR affinity and potency between EC-C225 and C225. Cellular uptake differed markedly between A431 and MDA231 cell lines. A431, a known EGFR expression cell line, showed higher uptake than did MDA231 (*24*).

Patient Eligibility

Patients with locally advanced squamous cell carcinomas of the head and neck who had been enrolled in a phase III trial (IMCL CP02-9815) and randomized to receive radiation therapy with concomitant C225 were eligible for this pilot study. This study (RO00-311) opened for patient accrual on January 16, 2001, and closed on April 5, 2002, after completion of the M.D. Anderson Cancer Center patient accrual goal for the phase III trial. During that interval, 8 patients were eligible for enrollment in RO00-311 but 2 declined participation.

Treatment Plan

^{99m}Tc-EC-C225 was administered during the morning of the day on which the 400 mg/m^2 loading dose of C225 was scheduled (every other patient entered on this protocol starting with patient 1 = arm 1) or immediately after the loading dose of C225 (every other patient entered on this protocol starting with patient 2 = arm 2). Just before injection of the ^{99m}Tc-EC-C225, a whole-body transmission scan using a ^{57}Co sheet source was obtained for every patient in arm 1, for attenuation correction of the ^{99m}Tc scans. To avoid delay between administration of the loading dose of C225 and administration of radiolabeled C225, patients in arm 2 underwent transmission scanning before administration of cold C225. At time 0, a mean of 925 MBq (range, 814–1,073 MBq) of ^{99m}Tc-EC-C225 was administered intravenously, immediately followed by the time 0 whole-body scan. With the exception of 1 patient (patient 5) who missed his 2-h scan because the camera was not available for research purposes, further whole-body scans were obtained at 2, 4, and 6 h after injection. To better assess renal dosimetry, the last 3 patients underwent whole-body imaging the morning after their injection of ^{99m}Tc-labeled C225. All patients voided immediately before the transmission scan and immediately before the scans obtained at 2, 4, 6, and 24 h after the time 0 injection.

The whole-body scans were obtained with a dual-detector γ-camera (e.cam; Siemens Medical Solutions USA, Inc.) over a scan length of 200 cm in approximately 20 min (10 cm/min), and the images were acquired into a 1,024 × 256 digital matrix. A board-certified attending nuclear medicine physician then read the images.

Radiation Dosimetry

The whole-body images were analyzed using the Nuclidose program (Northwestern University) to define regions of interest, construct time–activity curves, and estimate source organ residence times (*27*,*28*). For patient convenience, neither blood nor urine nor feces were collected in this phase I pilot study. Source organ fractions of injected activity versus time were computed from the serial anterior and posterior whole-body images using the geometric mean quantification method (*29*,*30*). First, attenuation correction factors were estimated from the ratio of organ region counts in a scan of the ^{57}Co sheet source without the patient to organ region counts in the transmission scan. The square root of this ratio was raised to the power μ_{140}/μ_{122} to convert to ^{99m}Tc attenuation, where μ_{140} and μ_{122} are the mass attenuation coefficients for ^{99m}Tc and ^{57}Co, respectively. The camera sensitivity was measured by including a 10-mL vial containing a calibrated reference source of activity within the field of view of each patient's whole-body scan. This sensitivity was then used to scale the ^{99m}Tc-emission organ region counts to convert them to absolute activity. Finally, for the fraction of injected activity in each source organ, the time–activity curve was fit to either a monoexponential or biexponential function, and the function was integrated analytically to calculate residence time. Estimates of the radiation-absorbed doses to the standard MIRD target organs were then computed using the MIRDOSE3 algorithms (*31*,*32*). In addition to absorbed dose estimates to the standard MIRD target organs, effective dose equivalent and effective dose were calculated. Source-organ residence times were estimated for the kidneys, liver, lungs, spleen, and remainder of the body. All other organs were considered targets of radiation only.

RESULTS

Labeling

The labeling was excellent at first but appeared to decline over the course of the study. For the first 2 patients, there was no significant visualization of the thyroid, stomach, salivary glands, or saliva (Fig. 1). For the third patient, there was no significant visualization of the stomach, salivary

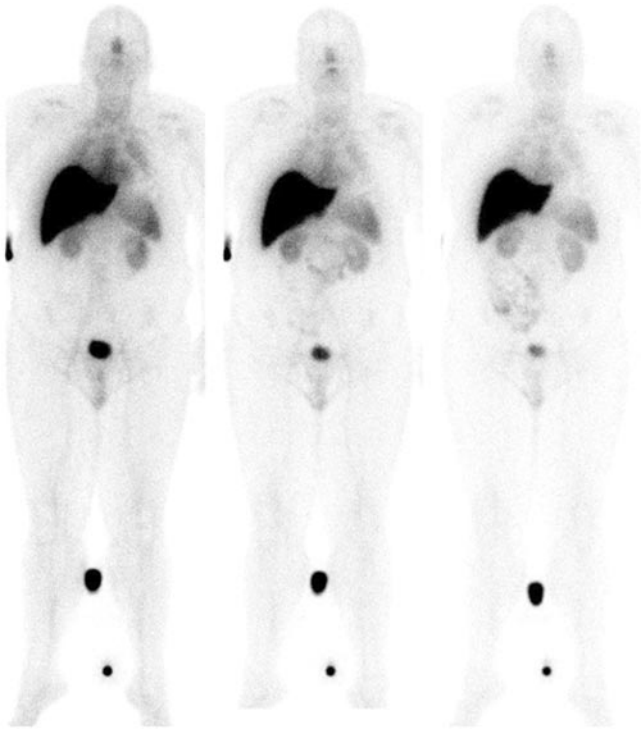

FIGURE 1. Whole-body coronal images obtained 2, 4, and 6 h (from left to right) after administration of 851 MBq of ^{99m}Tc-EC-C225 to a patient with squamous cell carcinoma of the head and neck—the first patient scanned with this compound.

glands, or saliva; however, the thyroid, which was not significantly visible at 2 h, became slightly visible at 4 h and more so at 6 h. For the fourth patient, there was no significant visualization of the stomach or saliva; however, there was mild visualization of the thyroid and salivary glands, suggesting the presence of some unlabeled free technetium or unstable labeled C225. For the fifth patient, there was no significant visualization of the thyroid or stomach, but there was some visualization of the salivary glands and saliva. The sixth patient's scan was suboptimal overall, with significant visualization of the thyroid, stomach, salivary glands, and saliva.

As an aside, the first patient's nasopharynx and fifth patient's gallbladder were well visualized. Delayed visualization of the nasopharynx and gastrointestinal system, after 4 h, was noted for patients 5 and 6.

Target-Organ Dosimetry

The critical organ was the kidney, with an average absorbed dose for all 6 patients of 0.1014 cGy/mCi (0.0274 mGy/MBq) ± 22.9%. The average total-body absorbed dose was 0.0081 cGy/mCi (0.0022 mGy/MBq; 0.243 cGy/1,110 MBq) ± 19.2%. Table 1 shows the average absorbed dose for all 6 patients; for the 3 patients in arm 1 (without cold loading), that is, patients 1, 3, and 5; for the 3 patients in arm 2 (with cold loading), that is, patients 2, 4, and 6; and

TABLE 1
Radiation Dosimetry: Mean Radiation Absorbed Dose for Each Target Organ ± SD (as % of Mean)

Target	Mean: all patients	Mean arm 1: without cold loading	Mean arm 2: with cold loading	Mean arm 2: without patient 6
Adrenals	0.0180 ± 30.3	0.0169 ± 39.0	0.0185 ± 33.3	0.0220 ± 7.1
Brain	0.0034 ± 33.3	0.0035 ± 32.3	0.0030 ± 36.0	0.0026 ± 40.1
Breasts	0.0108 ± 142.2	0.0044 ± 10.5	0.0044 ± 20.3	0.0047 ± 23.8
Gallbladder wall	0.0219 ± 53.2	0.0198 ± 71.6	0.0239 ± 47.5	0.0303 ± 11.9
Lower large intestine wall	0.0054 ± 25.9	0.0056 ± 25.5	0.0050 ± 26.2	0.0045 ± 31.4
Small intestine	0.0084 ± 10.0	0.0083 ± 9.9	0.0082 ± 15.3	0.0086 ± 16.9
Stomach	0.0108 ± 23.0	0.0111 ± 27.9	0.0103 ± 26.4	0.0116 ± 19.6
Upper large intestine wall	0.0094 ± 17.5	0.0091 ± 21.2	0.0094 ± 22.3	0.0104 ± 16.1
Heart wall	0.0098 ± 26.1	0.0095 ± 29.7	0.0100 ± 29.9	0.0115 ± 19.3
Kidneys	0.1014 ± 22.9	0.0891 ± 16.5	0.1010 ± 30.1	0.1107 ± 32.4
Liver	0.0582 ± 80.9	0.0504 ± 112.6	0.0675 ± 64.9	0.0923 ± 13.4
Lungs	0.0139 ± 27.0	0.0132 ± 26.0	0.0150 ± 28.4	0.0173 ± 12.7
Muscle	0.0059 ± 11.4	0.0059 ± 10.1	0.0057 ± 16.9	0.0059 ± 21.1
Ovaries	0.0061 ± 19.5	0.0063 ± 17.4	0.0057 ± 21.2	0.0054 ± 28.1
Pancreas	0.0184 ± 30.4	0.0183 ± 34.6	0.0182 ± 36.2	0.0218 ± 15.3
Red marrow	0.0067 ± 9.4	0.0066 ± 8.7	0.0065 ± 14.3	0.0068 ± 16.5
Bone surfaces	0.0106 ± 11.2	0.0106 ± 8.2	0.0102 ± 16.4	0.0104 ± 22.2
Skin	0.0035 ± 13.6	0.0036 ± 10.2	0.0033 ± 18.0	0.0033 ± 25.6
Spleen	0.0793 ± 83.5	0.0979 ± 92.0	0.0641 ± 59.5	0.0813 ± 41.2
Testes	0.0036 ± 32.9	0.0038 ± 31.8	0.0032 ± 35.1	0.0027 ± 39.7
Thymus	0.0055 ± 13.0	0.0056 ± 8.2	0.0054 ± 19.0	0.0054 ± 26.8
Thyroid	0.0120 ± 159.4	0.0198 ± 135.7	0.0192 ± 142.1	0.0035 ± 36.4
Bladder wall	0.0049 ± 28.5	0.0051 ± 27.0	0.0045 ± 30.3	0.0039 ± 35.7
Uterus	0.0060 ± 21.0	0.0062 ± 27.7	0.0056 ± 22.6	0.0052 ± 29.1
Total body	0.0081 ± 19.2	0.0079 ± 10.6	0.0081 ± 24.4	0.0091 ± 17.1

Data are in cGy/mCi (1 mCi = 37 MBq).

TABLE 2
Radiation Dosimetry: Residence Times ± SD (as % of Mean)

Target	Mean: all patients	Mean arm 1: without cold loading	Mean arm 2: with cold loading	Mean arm 2: without patient 6
Kidneys	0.50 ± 26.1	0.51 ± 25.0	0.50 ± 32.9	0.54 ± 17.0
Liver	1.25 ± 88.3	1.03 ± 132.6	1.47 ± 69.2	2.04 ± 7.6
Lungs	0.15 ± 20.4	0.13 ± 16.7	0.16 ± 19.9	0.18 ± 69.3
Spleen	0.23 ± 94.2	0.28 ± 110.4	0.18 ± 67.8	0.23 ± 220.1
Remainder of body	1.94 ± 34.0	2.14 ± 34.9	1.73 ± 36.3	1.46 ± 15.4

Data are in hours.

for the patients in arm 2 excluding patient 6. In Table 2, residence times are provided for the kidneys, liver, lungs, spleen, and remainder of the body.

Effective Dose Equivalent and Effective Dose

The mean effective dose equivalent for all 6 patients was 0.0222 cSv/mCi (0.006 mSv/MBq; 0.666 cSv/1,110 MBq) ± 24.3%. The mean effective dose for all 6 patients was 0.0138 cSv/mCi (0.004 mSv/MBq; 0.414 cSv/1,110 MBq) ± 15.5%. Table 3 shows the average effective dose equivalent and average effective dose for all 6 patients; for the 3 patients in arm 1 (without cold loading), that is, patients 1, 3, and 5; for the 3 patients in arm 2 (with cold loading), that is, patients 2, 4, and 6; and for the patients in arm 2 excluding patient 6.

DISCUSSION

Labeling was excellent overall, and at 90%–100%, radiochemical purity for ^{99m}Tc-EC-C225 was reasonable. Nine months transpired between administration of ^{99m}Tc-EC-C225 to the first patient and administration to the last patient. The seeming decline in labeling over that time may have been related to the second small peak (<10%) seen on HPLC at 7.5 min, consistent with the presence of a lower-molecular-weight antibody. The suboptimal study of the last patient was due to the accumulation of a significant amount of free ^{99m}Tc in the saliva and salivary glands; the presence of free ^{99m}Tc was corroborated by significant visualization of this patient's thyroid and stomach on a whole-body scan.

The dosimetric estimates and especially average absorbed dose to the critical organ (0.0274 mGy/MBq) and to the whole body (0.0022 mGy/MBq [0.243 cGy/1,110 MBq]) indicate that the new radiopharmaceutical ^{99m}Tc-EC-C225 has reasonable dosimetric properties for a diagnostic nuclear medicine agent.

We do not have sufficient patient numbers to make a strong recommendation on whether cold loading should be used. Residence time in the liver appeared to be longer in patients with cold loading than in those without. One explanation could be that the liver does not have C225 binding sites but simply extracts whatever is not taken up elsewhere in the body. If the cold loading saturates many potential binding sites elsewhere in the body—leaving fewer nonliver binding sites to be labeled with ^{99m}Tc-EC-C225—the result would be more activity in the liver. If this is true, one may hypothesize that cold loading would be disadvantageous for the imaging of tumors.

CONCLUSION

The new radiopharmaceutical ^{99m}Tc-EC-C225 appears to have dosimetric properties that are reasonable for a diagnostic nuclear medicine agent. For best results, we recommend the fresh synthesis of EC-C225 before radiolabeling and scanning. Because C225 therapy is directed against tumors, which express EGFR, the imaging of patients with ^{99m}Tc-EC-C225 could potentially select good candidates for C225 therapy trials.

ACKNOWLEDGMENTS

We are grateful for the dedicated efforts of our research nurse, Beth de Gracia; research assistant, Kristen Reynolds; and administrative assistants, Sylvia Kolojaco, Marie

TABLE 3
Radiation Dosimetry: Effective Dose Equivalent and Effective Dose ± SD (as % of Mean)

Parameter	Mean: all patients	Mean arm 1: without cold loading	Mean arm 2: with cold loading	Mean arm 2: without patient 6
Effective dose equivalent	0.0222 ± 24.3	0.0222 ± 27.7	0.0221 ± 28.1	0.0256 ± 8.0
Effective dose	0.0138 ± 15.5	0.0136 ± 10.6	0.0143 ± 16.7	0.0156 ± 10.5

Data are in cSv/mCi (1 mCi = 37 MBq).

Turner, and Eloise Daigle. This work was supported by a grant from ImClone Systems Inc.

REFERENCES

1. Grandis JR, Melheim MF, Gooding WE, et al. Levels of TGF-alpha and EFGr protein in head and neck squamous cell carcinoma and patient survival. *J Natl Cancer Inst.* 1998;90:824–832.
2. Dassonville O, Formento JL, Francoual M, et al. Expression of epidermal growth factor receptor and survival in upper aerodigestive tract cancer. *J Clin Oncol.* 1993;11:1873–1878.
3. O-charoenrat P, Rhys-Evans P, Modjtahedi H, et al. Overexpression of epidermal growth factor receptor in human head and neck squamous cell lines correlates with matrix metalloproteinase-9-expression and in vitro invasion. *Int J Cancer.* 2000;86:307–317.
4. Ozanne B, Richards CS, Hendler F, et al. Over-expression of the EGF receptor is a hallmark of squamous cell carcinomas. *J Pathol.* 1986;149:9–14.
5. Etienne MC, Pivot X, Formento JL, et al. A multifactorial approach including tumoural epidermal growth factor receptor, p53, thymidylate synthase and dihydropyrimidine dehydrogenase to predict treatment outcome in head and neck cancer patients receiving 5-fluorouracil. *Br J Cancer.* 1999;79:1864–1869.
6. Gullick WJ. Prevalence of aberrant expression of the epidermal growth factor receptor in human cancers. *Br Med Bull.* 1991;47:87–96.
7. Akimoto T, Hunter NR, Buchmiller L, et al. Inverse relationship between epidermal growth factor receptor expression and radiocurability of murine carcinomas. *Clin Cancer Res.* 1999;5:2884–2890.
8. Ang KK, Berkey BA, Tu X, et al. Impact of epidermal growth factor receptor on survival and pattern of relapse in patients with advanced head and neck cancer. *Cancer Res.* 2002;62:7350–7356.
9. Sato JD, Kawamoto T, Le AD, et al. Biological effects in vitro of MABs to human EGF receptors. *Mol Biol Med.* 1983;1:511–514.
10. Kawamoto T, Sato JD, Polikoff J, et al. Growth stimulation of A431 cells by EGF: identification of high affinity receptors for epidermal growth factor by an anti-receptor monoclonal antibody. *Proc Natl Acad Sci USA.* 1983;80:1337–1341.
11. Masui H, Moroyama T, Mendelsohn J. Mechanism of anti-tumor activity in mice for anti-epidermal growth factor receptor monoclonal antibodies with different isotypes. *Cancer Res.* 1986;46:5592–5598.
12. Fan Z, Masui H, Mendelsohn J. Blockade of epidermal growth factor receptor function by bivalent and monoclonal fragments of 225 anti-epidermal growth factor monoclonal antibodies. *Cancer Res.* 1993;53:4322–4328.
13. Khazaeli MB, Conry RM, LoBuglio AF. Human immune response to monoclonal antibodies. *J Immunother.* 1994;15:42–52.
14. Kuus-Reichel K, Grauer LS, Karavodin LM, et al. Will immunogenicity limit the use, efficacy, and future development of therapeutic monoclonal antibodies? *Clin Diagn Lab Immunol.* 1994;1:365–372.
15. Goldstein NI, Prewett M, Zuklys K, et al. Biological efficacy of a chimeric antibody to the epidermal growth factor receptor in a human tumor xenograft model. *Clin Cancer Res.* 1995;1:1311–1318.
16. Huang S, Li J, Harari PM. Molecular inhibition of angiogenesis and metastatic potential in human squamous cell carcinomas after epidermal growth factor receptor blockade. *Mol Cancer Ther.* 2002;1:507–514.
17. Bonner JA, Raish KP, Trummell HQ, et al. Enhanced apoptosis with combination C225/radiation treatment serves as the impetus for clinical investigation in head and neck cancers. *J Clin Oncol.* 2000;18:47s–53s.
18. Busam KJ, Capodieci P, Motzer R, et al. Cutaneous side-effects in cancer patients treated with the anti-epidermal growth factor receptor antibody C225. *Br J Dermatol.* 2001;144:1169–1176.
19. Nasu S, Ang KK, Fan Z, et al. C225 anti-epidermal growth factor receptor antibody enhances tumor radiocurability. *Int J Rad Oncol Biol Phys.* 2001;51:474–477.
20. Mendelsohn J. The epidermal growth factor receptor as a target for cancer therapy. *Endocr Relat Cancer.* 2001;8:3–9.
21. Ford AC, Grandis JR. Targeting epidermal growth factor receptor in head and neck cancer. *Head Neck.* 2003;25:67–73.
22. Herbst RS, Langer CJ. Epidermal growth factor receptors as a target for cancer treatment: the emerging role of IMC-C225 in the treatment of lung and head and neck cancers. *Semin Oncol.* 2002;1:27–36.
23. Baselga J. Why the epidermal growth factor receptor? The rationale for cancer therapy. *Oncologist.* 2002;7:2–8.
24. Schechter NR, Yang DJ, Azhdarinia A, et al. Assessment of epidermal growth factor receptor with ^{99m}Tc-ethylenedicysteine-C225 monoclonal antibody. *Anticancer Drugs.* 2003;1:49–56.
25. Blondeau P, Berse C, Gravel D. Dimerization of an intermediate during the sodium in liquid ammonia reduction of L-thiazolidine-4-carboxylic acid. *Can J Chem.* 1967;45:49–52.
26. Ratner S, Clarke HT. The action of formaldehyde upon cysteine. *J Am Chem Soc.* 1937;59:200–206.
27. Erwin WD, Groch MW, Spies SM. Development of a quantitative imaging and MIRD dosimetry software application for radionuclide therapy treatment planning using a fourth generation language [abstract]. *Radiology.* 1997;205(suppl):261.
28. Erwin WD, Groch MW, Spies SM, et al. Clinical validation of a quantitative imaging and MIRD dosimetry software application: retrospective application to anti-B-cell lymphoma MAB studies [abstract]. *Clin Nucl Med.* 1998;23:561.
29. Erwin WD, Groch MW, Macey DJ, et al. A radioimmunoimaging and MIRD dosimetry treatment planning program for radioimmunotherapy. *Nucl Med Biol.* 1996;23:525–532.
30. Siegel JA, Thomas SR, Stubbs JB, et al. MIRD pamphlet no. 16: techniques for quantitative radiopharmaceutical biodistribution data acquisition and analysis for use in human radiation dose estimates. *J Nucl Med.* 1999;40(suppl):37S–61S.
31. Loevinger R, Budinger TF, Watson E, et al. *MIRD Primer for Absorbed Dose Calculations*. Revised ed. New York, NY: The Society of Nuclear Medicine, Inc.; 1991:5–10.
32. Stabin MG. MIRDOSE: personal computer software for internal dose assessment in nuclear medicine. *J Nucl Med.* 1996;37:538–546.